Biosensors and Bioelectronics 86 (2016) 454–458

Contents lists available at ScienceDirect

Biosensors and Bioelectronics

journal homepage: www.elsevier.com/locate/bios

Ultrasensitive electrochemical detection of miRNA-21 by using an iridium(III) complex as catalyst

Xiangmin Miao [a,b], Wanhe Wang [b], Tianshu Kang [c], Jinbiao Liu [b], Kwok-Keung Shiu [b], Chung-Hang Leung [c], Dik-Lung Ma [b,*]

[a] School of Life Science, Jiangsu Normal University, Xuzhou 221116, PR China
[b] Department of Chemistry, Hong Kong Baptist University, Kowloon Tong, Hong Kong, China
[c] State Key Laboratory of Quality Research in Chinese Medicine, Institute of Chinese Medical Sciences, University of Macau, Macao, China

ARTICLE INFO

Article history:
Received 5 May 2016
Received in revised form
27 June 2016
Accepted 1 July 2016
Available online 2 July 2016

Keywords:
Iridium(III) complex
miRNA-21
Electrochemical biosensor

ABSTRACT

The ultrasensitive electrochemical detection of miRNA-21 was realized by using a novel redox and catalytic "all-in-one" mechanism with an iridium(III) complex as a catalyst. To construct such a sensor, a capture probe (CP) was firstly immobilized onto the gold electrode surface. In the presence of miRNA-21, a sandwiched DNA complex could form between CP and a methylene blue (MB) labeled G-rich detection probe modified onto a gold nanoparticle (AuNP) surface (DP-AuNPs). Upon addition of K^+, the structure of DP changed to a G-quadruplex. Then, the iridium(III) complex could selectively interact with the G-quadruplex, catalyzing the reduction of H_2O_2, which was accompanied by an electrochemical signal change using MB as an electron mediator. Under optimal conditions, the electrochemical signal of MB reduction peak was proportional to miRNA concentration in the range from 5.0 fM to 1.0 pM, with a detection limit of 1.6 fM. In addition, satisfactory results were obtained for miRNA-21 detection in human serum samples, indicating a potential application of the sensor for bioanalysis.

1. Introduction

miRNAs are a group of short (approximately 22 nucleotides) and endogenously expressed noncoding RNAs, which play crucial roles in biological and cellular processes (Hong et al., 2014). Aberrant miRNA expression is directly associated with several diseases such as cancer, diabetes, cardiovascular disease and neurological disorders (Cissell et al., 2008; Esquela-Kerscher and Slack, 2006). Additionally, miRNAs have been utilized as potential biomarkers in clinical diagnostics and as targets for disease therapy. Thus, developing highly sensitive strategies for miRNA detection is of great importance in biology and medicine. In recent decades, numerous analytical strategies including electrochemical (Chen et al., 2015; Li et al., 2015a, 2015b; Ren et al., 2013; Tran et al., 2014), fluorescent (Causa et al., 2015; Degliangeli et al., 2014; Lin et al., 2015; Wang et al., 2015a), colorimetric (Dong et al., 2015; Park et al., 2014; Shen et al., 2013; Wang et al., 2014), surface plasmon resonant (Li et al., 2016; Zheng et al., 2015) and electrochemiluminescent (Yu et al., 2014; Zhang et al., 2015) platforms have been reported for miRNA detection. Of those, electrochemical-based systems enjoy intrinsic advantages because of their simplicity, easy miniaturization, low cost and high sensitivity (Cheng et al., 2009; Deng et al., 2014; Liu et al., 2013; Rafiee-Pour et al., 2016; Wen et al., 2012).

Recently, redox cycling-based catalytic strategies have received considerable attention in electrochemical biosensor preparation. In such a strategy, electrochemically oxidized (or reduced) species are reduced (or oxidized), the regenerated electroactive species are electrochemically re-oxidized (or re-reduced), resulting in high electrochemical signals. For example, Tang's group developed an electrochemical immunosensor for tumor marker detection by using a redox-catalysis 'all-in-one' mechanism (Zhang et al., 2015a). Liu et al. realized the electrochemical detection of miRNAs based on the signal amplification of gold nanoparticles (AuNPs), enzymes and redox-cycling (Liu et al., 2014). In this context, artificial peroxidase mimics have received wide attention as an alternative to proteinous peroxidases due to their simple preparation, low price and good stability, which can avoid the drawbacks of peroxidases such as cost-ineffectiveness, environmental instability, and difficult purification for practical applications (Dong et al., 2016). So far, a variety of inorganic nanomaterials such as Fe_3O_4 or Fe_2O_3 nanoparticles (Gao et al., 2007; Roy et al., 2016), metal nanoparticles (Ahmed et al., 2016; Xia et al., 2015; Zhang et al., 2015b) and carbon-based nanomaterials (Liu et al., 2012; Song et al., 2010) have been reported as peroxidase mimics for biosensor preparation. However, to the best of our knowledge, no

* Corresponding author.
E-mail address: edmondma@hkbu.edu.hk (D.-L. Ma).

http://dx.doi.org/10.1016/j.bios.2016.07.001
0956-5663/

analytical detection has yet been developed by using an iridium (III) complex as a peroxidase mimics catalyst.

Herein, we report for the first time a sensitive redox and catalytic "all-in-one" sensing platform for miRNA-21 detection by employing an iridium(III) complex as a peroxidase-like mimic, which directly avoid the drawbacks of enzyme-involved electrocatalytic amplification assays. In addition, iridium(III) complexes could selectively interact with G-quadruplex DNA structures (Lin et al., 2015; Ma et al., 2015a, 2015b; Mao et al., 2016; Wang et al., 2015b, 2016; Leung et al., 2011; Lu et al., 2014), making our method relatively low-cost. Although the use of metal nanoparticles has triggered concern due to their potential toxicity (Chen et al., 2009), AuNPs have been shown to be relatively harmless to human cells (Chen et al., 2009; Paciotti et al., 2004) and possess high surface area and good biocompatibility, thus making them attractive for biosensor preparation. Here, AuNPs were used to immobilize large numbers of G-quadruplex DNA species, which greatly amplified the electrochemical signal. Importantly, our method avoids the instability and high cost of proteinous enzymes, as well as the tedious labeling of nanoparticles.

2. Experimental section

2.1. Reagent and chemicals

6-Mercapto-1-hexanol (MCH), sodium citrate, and gold chloride ($HAuCl_4$) were purchased from Sigma Aldrich (St. Louis, MO). Other chemicals and solvents used in the experiment were of analytical grade. 20.0 mM of tris-buffer (pH 7.0) was used for miRNA detection and 20.0 mM of tris-buffer (pH 7.0, with 50 mM K^+) was used for G-quadruplex formation. Human serum samples that used for the addition and recovery experiments of miRNA-21 were purchased from Sigma Aldrich (St. Louis, MO), and diluted 100 times before using.

All oligonucleotides were synthesized by Techdragon Inc. (Hong Kong, China), and the sequences of the oligonucleotides were as follows:

Capture probe (CP): 5′- CTGATAAGCTATCGACTA-$(CH_2)_6$-SH-3′.

Target miRNA-21: 5′-UAGCUUAUCAGACUGAUGUUGA-3′.

Detection probe (DP): 5′-SH-$(CH_2)_6$-TCAGACACTCAA-CATCAGGGACAGGG CTACAGGGTCAGGG-MB-3′.

The structure of the iridium(III) complex $[Ir(ppy)_2(dpq)]PF_6$ was shown in Fig. 1, and we have previously demonstrated its ability to selectively interact with G-quadruplex DNA (Ma et al., 2015a). This iridium(III) complex was synthetized according to the literature method (Lo et al., 2006).

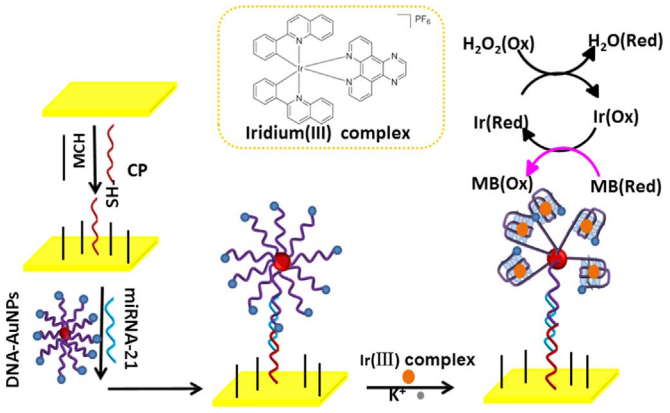

Fig. 1. Schematic diagram for the electrochemical detection of miRNA-21.

2.2. miRNA-21 detection protocol

Before modification, gold electrodes were pretreated according to our previous method (Li et al., 2015a, 2015b). Then, the pretreated gold electrodes were incubated in 20 mM of tris-buffer (pH 7.0) containing 5.0 μM of CP for 16 h at room temperature (RT), followed by reacting with 1.5 μM of MCH for 1.5 h to block nonspecific sites. After that, the modified electrodes were immersed into a solution containing different concentration of miRNA-21 and 1.0 μM of DP-AuNPs probe and the mixture was incubated for 30 min at RT. Subsequently, the modified electrodes were incubated in 20 mM of tris-buffer (pH 7.0, with 50 mM K^+) and 3.0 μM of iridium(III) complex for another 45 min to induce the formation of G-quadruplex and the selective interaction of the iridium(III) complex. Finally, the electrochemical characteristics of the sensor were investigated in tris-buffer containing 1.0 μM of H_2O_2 by using cyclic voltammetry (CV) at RT.

3. Results and discussion

3.1. Mechanism of the miRNA-21 sensor

As shown in Fig. 1, the capture probe (CP) was immobilized onto the gold electrode surface based on Au-S chemistry. In the presence of miRNA-21, a sandwiched DNA complex could form between CP and the DP-AuNPs probe, and the G-rich region of DP-AuNPs could transform into a G-quadruplex structure upon the presence of K^+, followed by the specific interaction of iridium(III) complex with G-quadruplex DNA. Then, upon addition of 1.0 μM H_2O_2 in the detection solution, the iridium(III) complex immobilized on the electrode can catalyze the reduction of H_2O_2. A possible catalysis mechanism may involve the oxidation of Ir $(ppy)_2(dpq)^{3+}$ to $Ir(ppy)_2(dpq)^{4+}$ by using H_2O_2 as an oxidant, resulting in the electron transfer. A redox peak signal change could then be realized by using MB as a reversible electron mediator. We found that the signal change of MB was directly dependent on the concentration of iridium(III) complex that interacted with G-quadruplex DNA, and therefore indirectly associated with the concentration of miRNA-21. Thus, by calculating the variation of the MB reduction peak, miRNA-21 concentration could be quantitatively evaluated.

The relationship between the CV scan rate and the peak current of MB was also studied in the range of 5–500 mV/s. As shown in Fig. S1A, a pair of well-defined redox peaks appeared at different scan rates and the redox peak currents were increased along with the increase of scan rates, and good linear relations were obtained between the redox peak current and the square root of scan rate (Fig. S1B). Meanwhile, a good relationship of $\ln I_{peak}$ with $\ln_{rate}$ was obtained with linear regression equations $\ln I_{peak(Ox)}=0.5287\ln_{rate}$ (mV/s)+2.0662 ($R^2=0.997$) and $I_{peak(Red)}=0.4976\ \ln_{rate}$ (mV/s)+ 2.2079 ($R^2=0.999$), respectively. The slope value of 0.5287 and 0.4976 were close to the theoretical value of 0.5. According to the literature (Hasanzadeh et al., 2009, 2014; Soleymani et al., 2016; Sun et al., 2012), our sensor reaction was a diffusion-controlled process.

In our sensor, the peak currents of MB increased along with an increase of the scan rate, which indicated that the electron-transfer between MB and the electrode surface was mediated by the sandwiched CP/miRNA/DP complex via a diffusion-controlled process. Meanwhile, the oxidation peak potential of MB shifted to a positive value while the reduction peak potential shifted to a negative value as the scan rate increased. This change of the redox peak of MB directly indicates the occurrence of the heterogeneous electron-transfer reaction of MB on the modified electrode surface (Farjami et al., 2011; Rafiee-Pour et al., 2016).

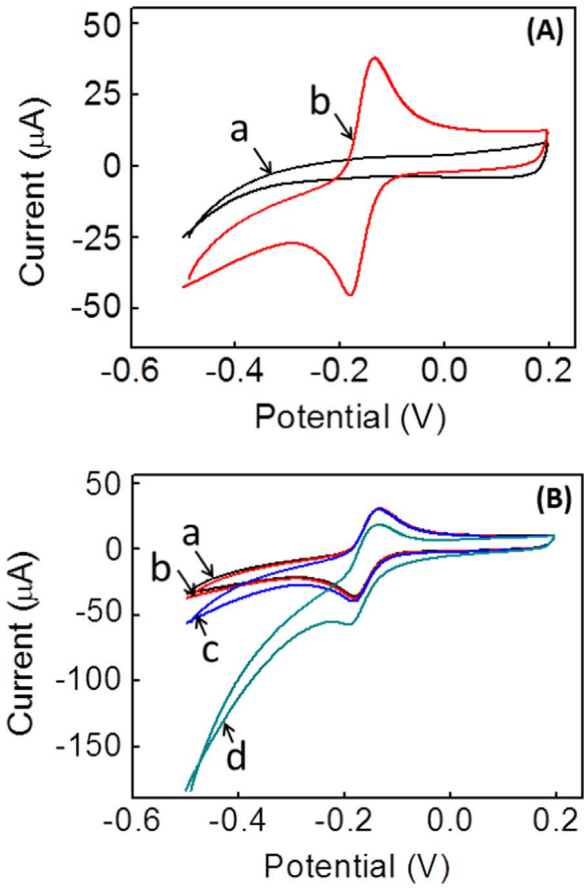

Fig. 2. (A) CV curves of (a) bare gold electrode and (b) the sandwiched DNA complex modified gold electrode obtained in 20 mM of tris-buffer (pH 7.0, with 50 mM of K^+) containing 10 fM of miRNA-21; (B) CV curves of different modified electrodes obtained in 20 mM of tris-buffer (pH 7.0, with 50 mM of K^+) containing 10 fM of miRNA-21: (a) sandwiched DNA complex modified gold electrode, (b) a after the interaction with iridium complex, (c) a in the presence of 1.0 μM of H_2O_2 and (d) b in the presence of 1.0 μM of H_2O_2.

3.2. Characterization of the sensor

To further prove the effective formation of the sandwiched DNA complex, different modified electrodes were investigated by CV experiments. As shown in Fig. 2A, there was an obvious redox peak of MB on the sandwiched DNA complex modified gold electrode (curve b) compared to the bare electrode (curve a) in the presence of 10 fM of miRNA-21. The electrochemical detection of miRNA-21 was performed based on observing the current signal change (ΔI) of MB reduction peak. As shown in Fig. 2B, a well redox peak of MB was observed in the presence of 10 fM of miRNA-21 due to the formation of the sandwiched DNA complex on the electrode surface (curve a). Additionally, the interaction of the iridium(III) complex with DP in the absence of H_2O_2 did not affect the redox peak of MB (curve b). However, upon the addition of 1.0 μM of H_2O_2, the reduction peak of MB largely increased (curve d) compared with the results of without interacting of iridium(III) complex with sandwiched DNA complex (curve c). Compared to curve "a", the slight increase of the reduction peak of MB in curve "c" might be due to the decomposition and reduction of H_2O_2 itself while the obvious increase in the reduction peak of MB indicated that the iridium(III) complex could catalyze the reduction of H_2O_2 after its selective interaction with DP.

3.3. Peroxidase-like activity of iridium(III) complex

By using no MB labeled DP-AuNPs for iridium(III) complex immobilization, an obvious catalytic current also appeared along with the increase of H_2O_2 concentration from 1.0 μM to 3.0 μM (Fig. S2B). Such results revealed that the iridium(III) complex has good catalytic ability for the reduction of H_2O_2. Meanwhile, the peroxidase-like activity of the iridium(III) complex was also investigated through a colorimetric reaction by using H_2O_2 to oxidize TMB (Xia et al., 2015; Zhang et al., 2014b), a colorless peroxidase substrate. As shown in Fig. S3, an obvious color change of TMB from colorless to green could be observed, indicating that the iridium(III) complex could catalyze the oxidation of TMB substrate with H_2O_2.

In addition, to confirm that the catalytic mechanism of iridium (III) complex for H_2O_2 was due to the oxidation of Ir(III) to Ir(IV), different iridium(III) complexes were synthesized (Fig. S4). The catalytic capability of these complexes for H_2O_2 was studied (Fig. S2D), and it could be seen that the catalytic currents were similar in the presence of 1.0 μM H_2O_2, suggesting that the catalysis of H_2O_2 was mainly determined by the valence state change of iridium(III) center, rather than the CN or NN ligands, as is consistent with literature (You et al., 2004).

3.4. Performance of the sensor

Under optimal conditions, the sensitivity of the sensor for miRNA-21 detection was evaluated with CV experiments in tris-buffer (20 mM, pH 7.0, with 50 mM of K^+) containing 1.0 μM of H_2O_2. The current signal of the MB reduction peak increased linearly along with the increase of miRNA-21 concentration in the range from 5.0 fM to 1.0 pM (Fig. 3A). From the dose-response curve (Fig. 3B) and the calibration curve (inset of Fig. 3B, linear a), a detection limit of 1.6 fM (3σ) and a limit of quantity of 3.4 fM was obtained. The linear regression equation was $I = -50.18 - 74.49c$ (c:pM) with a correlation coefficient of $R^2 = 0.996$. Meanwhile, the redox peak potential of MB shifted along with increased miRNA concentration, which we attributed to the change of the electrode surface with increasing miRNA concentration, thereby affecting the electron-transfer and the redox reversibility of MB, as has been reported in the literature (Rafiee-Pour et al., 2016; Sun et al., 2012). For comparison, the current response of the sensor was recorded without G-quadruplex DNA. The current of the MB reduction peak increased along with the increase of miRNA-21 concentration in the range from 100 fM to 1.0 pM, which was mainly due to the quantitative increase of MB immobilized on the electrode (inset of Fig. 3B, linear b). The high sensitivity of the sensor might be attributed to two factors: the first is the amplification of the amount of immobilized DPs due to the use of the large surface area of AuNPs, leading to a greater quantity of iridium(III) complex that can be bound by the G-quadruplex DNA; The second is the high electro-catalytic activity of the iridium(III) complex towards H_2O_2. In addition, the sensitivity of our method was compared with other methods in Table S1, the detection limit of our detection platform was comparable with other electrochemical methods for miRNA-21 detection (Liu et al., 2014, 2015; Wu et al., 2014; Yin et al., 2012), which may be attributed to two factors: Although the sensitivity of the sensor was lower than some other electrochemical methods (Ren et al., 2013; Zhang et al., 2014a), the proposed method was suitable for biomolecular detection because it without needing the use of the enzyme.

3.5. Selectivity, repeatability, reproducibility and stability of the sensor

The selectivity of the sensor for miRNA-21 detection was investigated by monitoring the current signal change of the MB reduction peak in tris-buffer (20 mM, pH 7.0). As shown in Fig. S6A, the ΔI of MB reduction peak for 50 fM of miRNA-21 was

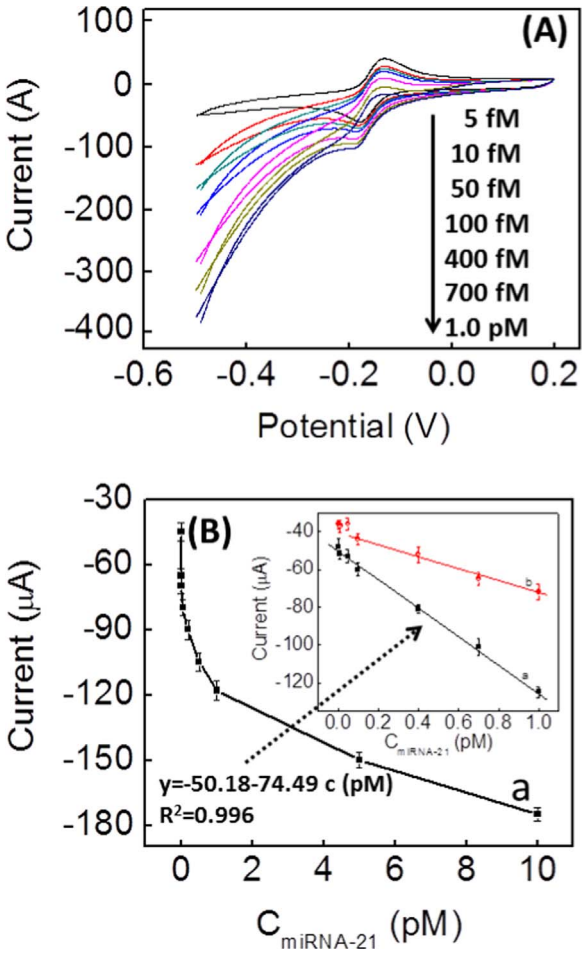

Fig. 3. CV experiments for miRNA-21 detection in 20 mM of tris-buffer solution (pH 7.0, with 50 mM of K^+) containing 1.0 μM of H_2O_2 (miRNA-21 concentration from up to down: 5 fM, 10 fM, 50 fM, 100 fM, 400 fM, 700 fM, 1.0 pM); (B) Dose-response curve and calibration curve (inset) for miRNA-21 detection (curve a: the proposed sensor, and curve b: the sensor without the selectively interaction of iridium(III) complex.

significantly greater than 50 pM (1000-fold excess) of other types of miRNAs, cysteine and BSA. This result demonstrates that the proposed sensor has high selectivity for miRNA-21 detection. Additionally, the repeatability of the sensor was investigated by using five sensors, and the results shown that closed current response to 10 fM of miRNA-21 was obtained with a relative standard deviation (RSD) of 3.12%, indicating a good repeatability of the sensor for miRNA-21 detection. In addition, a RSD of 5.8% for miRNA-21 detection was obtained over 12 repeats using the same sensor, while a RSD of 6.8% was obtained by using the same batch of electrodes, indicating that the sensor has an acceptable reproducibility for miRNA detection.

To study the stability of the sensor, CV experiments were executed conducted in continuous scanning mode in tris-buffer that contained 5 fM of miRNA-21. As shown in Fig. S6B, a RSD of 0.67% was obtained after continuous CV scans for 12 cycles. In addition, the stored stability of the sensor was also studied over one day and one month periods. The RSD for 12 measurements of 10 fM miRNA-21 with the same sensor was 5.37% (once an hour), indicating good precision of the sensor for miRNA-21 detection. Moreover, the sensor was stored at 4 °C for a 30-day period, and after the 5th, 10th, 15th, 20th, 25th and 30th days, 99.1%, 98.2%, 97.8%, 97.3%, 96.9% and 96.4%, respectively, of the initial intensity were preserved. Thus, the experimental results showed that the proposed sensor had excellent stability.

Table 1
Detection of miRNA-21 in human serum samples (n=5).

Sample	Added (fM)	Found (fM)	Recovery (%)	RSD (%)
1	10	10.6	106	3.26
2	50	48.3	96.6	2.18
3	100	97.2	97.2	4.13
4	500	512	102.4	2.56
5	1.0	1.08	108	3.09

3.6. miRNA-21 detection in human serum samples

To evaluate the application of our detection platform for miRNA-21 detection in human serum samples. Then, recovery experiments were conducted by using the standard addition method by adding 10, 50, 100, 500 and 1000 fM of miRNA-21 to human serum samples. As shown in Table 1, a good recovery in the range of 96.6–108% was observed, while the relative standard deviation (RSD) was below 4.13%, indicating that the proposed sensing platform can be potentially applied to monitor miRNA-21 in complex biological samples.

4. Conclusion

In conclusion, we have developed a sensitive platform for miRNA-21 detection based on a novel redox and catalytic “all-in-one” mechanism with a iridium(III) complexes a catalyst. This assay has several merits compared with conventional sensing strategies. First, the iridium(III) complex acts as a peroxidase-like mimic, which avoids issues associated with the instability and high cost of proteinous enzymes. In addition, the iridium(III) complex used in our method could selectively and stably interact with G-quadruplex DNA, making our method stable for miRNA-21 detection. Finally, the use of AuNPs with high surface area and good biocompatibility allowed for the amplification of the electrochemical signal as more G-quadruplex DNA structures could be immobilized. Thus, this assay is a promising technique for miRNA-21 detection in biological samples.

Acknowledgements

This work is supported by Hong Kong Baptist University (FRG2/14-15/004 and FRG2/15-16/002), the Health and Medical Research Fund (HMRF/14130522), the Research Grants Council (HKBU/201811, HKBU/204612, and HKBU/201913), the French Agence Nationale de la Recherche/Research Grants Council Joint Research Scheme (AHKBU201/12; Oligoswitch ANR-12-IS07-0001), the National Natural Science Foundation of China (21575121), the Guangdong Province Natural Science Foundation (2015A030313816), the Hong Kong Baptist University Century Club Sponsorship Scheme 2015, the Interdisciplinary Research Matching Scheme (RC-IRMS/14-15/06), the Science and Technology Development Fund, Macao SAR (098/2014/A2), and the University of Macau (MYRG091(Y3-L2)-ICMS12-LCH, MYRG2015-00137-ICMS-QRCM, and MRG044/LCH/2015/ICMS).

Appendix A. Supplementary material

Supplementary data associated with this article can be found in the online version at http://dx.doi.org/10.1016/j.bios.2016.07.001.

References

Ahmed, S.R., Kim, J., Suzuki, T., Lee, J., Park, E.Y., 2016. Biotechnol. Bioeng. . http://dx.doi.org/10.1002/bit.25982

Causa, F., Aliberti, A., Cusano, A.M., Battista, E., Netti, P.A., 2015. J. Am. Chem. Soc. 137, 1758–1761.

Chen, A., Gui, G.F., Zhuo, Y., Chai, Y.Q., Xiang, Y., Yuan, R., 2015. Anal. Chem. 87, 6328–6334.

Chen, Y.S., Hung, Y.C., Liau, I., Huang, G.S., 2009. Nanoscale Res. Lett. 4, 858–864.

Cissell, K.A., Rahimi, Y., Shrestha, S., Hunt, E.A., Deo, S.K., 2008. Anal. Chem. 80, 2319–2325.

Cheng, Y., Zhang, X., Li, Z., Jiao, X., Wang, Y., Zhang, Y., 2009. Angew. Chem. 121, 3318–3322.

Deng, R., Tang, L., Tian, Q., Wang, Y., Lin, L., Li, J., 2014. Angew. Chem. Int. Ed. 53, 2389–2393.

Degliangeli, F., Kshirsagar, P., Brunetti, V., Pompa, P.P., Fiammengo, R., 2014. J. Am. Chem. Soc. 136, 2264–2267.

Dong, H., Meng, X., Dai, W., Cao, Y., Lu, H., Zhou, S., Zhang, X., 2015. Anal. Chem. 87, 4334–4340.

Dong, M., Zhang, L., Li, R., Li, S., Jiang, Y., Qiao, Y., Duan, Z., Li, R., Wang, Q., Wang, H., 2016. RSC Adv. 6, 47595–47599.

Esquela-Kerscher, A., Slack, F.J., 2006. Nat. Rev. Cancer 6, 259–269.

Farjami, E., Clima, L., Gothelf, K., Ferapontova, E.E., 2011. Anal. Chem. 83, 1594–1602.

Gao, L., Zhuang, J., Nie, L., Zhang, J., Zhang, Y., Gu, N., Wang, T., Feng, J., Yang, D., Perrett, S., 2007. Nat. Nanotechnol. 2, 577–583.

Hong, C.Y., Chen, X., Li, J., Chen, J.H., Chen, G., Yang, H.H., 2014. Chem. Commun. 50, 3292–3295.

Hasanzadeh, M., Karim-Nezhad, G., Shadjou, N., Hajjizadeh, M., Khalilzadeh, B., Saghatforoush, L., Abnosi, M.H., Babaei, A., Ershad, S., 2009. Anal. Biochem. 389, 130–137.

Hasanzadeh, M., Shadjou, N., Eskandani, M., Soleymani, J., Jafari, F., de la Guardia, M., 2014. Trac. Trend Anal. Chem. 53, 137–149.

Leung, C.H., Chan, D.S.H., Man, B.Y.W., Wang, C.J., Lam, W., Cheng, Y.C., Fong, W.F., Siu, W.W.L., Ma, D.L., 2011. Anal. Chem. 83, 463–466.

Li, Z., Miao, X., Xing, K., Zhu, A., Ling, L., 2015a. Biosens. Bioelectron. 74, 687–690.

Lin, S., Gao, W., Tian, Z., Yang, C., Lu, L., Mergny, J.L., Leung, C.H., Ma, D.L., 2015. Chem. Sci. 6, 4284–4290.

Liu, L., Song, C., Zhang, Z., Yang, J., Zhou, L., Zhang, X., Xie, G., 2015. Biosens. Bioelectron. 70, 351–357.

Liu, M., Zhao, H., Chen, S., Yu, H., Quan, X., 2012. ACS Nano 6 (4), 3142–3151.

Liu, H., Li, L., Duan, L., Wang, X., Xie, Y., Tong, L., Wang, Q., Tang, B., 2013. Anal. Chem. 85, 7941–7947.

Liu, L., Xia, N., Liu, H., Kang, X., Liu, X., Xue, C., He, X., 2014. Biosens. Bioelectron. 53, 399–405.

Lo, K.K.W., Chung, C.K., Zhu, N., 2006. Chem. Eur. J. 12, 1500–1512.

Li, J., Lei, P., Ding, S., Zhang, Y., Yang, J., Cheng, Q., Yan, Y., 2016. Biosens. Bioelectron. 77, 435–441.

Li, C., Wang, H., Shen, J., Tang, B., 2015d. Anal. Chem. 87, 4283–4291.

Lu, L.H., He, H.Z., Chan, D.S.H., Leung, C.H., Ma, D.L., 2014. Chem. Sci. 5, 4561–4568.

Ma, D.L., Lin, S., Lu, L., Wang, M., Hu, C., Liu, L.J., Ren, K., Leung, C.H., 2015a. J. Mater. Chem. B 3, 4780–4785.

Ma, D.L., Wang, M., He, B., Yang, C., Wang, W., Leung, C.H., 2015b. ACS Appl. Mater. Int. 7, 19060–19067.

Mao, Z., Wang, M., Liu, J., Liu, L.-J., Lee, S.M.Y., Leung, C.H., Ma, D.L., 2016. Chem. Commun. 52, 4450–4453.

Park, J., Yeo, J.S., 2014. Chem. Commun. 50, 1366–1368.

Paciotti, G.F., Myer, L., Weinreich, D., Goia, D., Pavel, N., McLaughlin, R.E., Tamarkin, L., 2004. Drug Deliv. 11, 169–183.

Rafiee-Pour, H.A., Behpour, M., Keshavarz, M., 2016. Biosens. Bioelectron. 77, 202–207.

Ren, Y., Deng, H., Shen, W., Gao, Z., 2013. Anal. Chem. 85, 4784–4789.

Roy, A., Sahoo, R., Ray, C., Dutta, S., Pal, T., 2016. RSC Adv. 6, 32308–32318.

Soleymani, J., Hasanzadeh, M., Shadjou, N., Jafari, M.K., Gharamaleki, J.V., Yadollahi, M., Jouyban, A., 2016. Mat. Sci. Eng. C 61, 638–650.

Song, Y., Wang, X., Zhao, C., Qu, K., Ren, J., Qu, X., 2010. Chem. Eur. J. 16, 3617–3621.

Sun, W., Wang, Y., Zhang, Y., Ju, X., Li, G., Sun, Z., 2012. Anal. Chim. Acta 751, 59–65.

Shen, W., Deng, H., Ren, Y., Gao, Z., 2013. Chem. Commun. 49, 4959–4961.

Tran, H., Piro, B., Reisberg, S., Nguyen, L.H., Nguyen, T.D., Duc, H., Pham, M., 2014. Biosens. Bioelectron. 62, 25–30.

Wang, W., Kong, T., Zhang, D., Zhang, J., Cheng, G., 2015a. Anal. Chem. 87, 10822–10829.

Wang, S., Fu, B., Wang, J., Long, Y., Zhang, X., Peng, S., Guo, P., Tian, T., Zhou, X., 2014. Anal. Chem. 86, 2925–2930.

Wen, Y., Xu, Y., Mao, X., Wei, Y., Song, H., Chen, N., Huang, Q., Fan, C., Li, D., 2012. Anal. Chem. 84, 7664–7669.

Wang, M., Wang, W., Kang, T.S., Leung, C.H., Ma, D.L., 2015b. Anal. Chem. 88, 981–987.

Wang, W., Mao, Z., Wang, M., Liu, L.J., Kwong, D.W., Leung, C.H., Ma, D.L., 2016. Chem. Commun. 52, 3611–3614.

Wu, X., Chai, Y., Yuan, R., Zhuo, Y., Chen, Y., 2014. Sens. Actuators B: Chem. 203, 296–302.

Xia, X., Zhang, J., Lu, N., Kim, M.J., Ghale, K., Xu, Y., McKenzie, E., Liu, J., Ye, H., 2015. ACS Nano 9, 9994–10004.

Yin, H., Zhou, Y., Zhang, H., Meng, X., Ai, S., 2012. Biosens. Bioelectron. 33, 247–253.

You, T., Niwa, O., Kurita, R., Iwasaki, Y., Hayashi, K., Suzuki, K., Hirono, S., 2004. Electroanalytical 16, 54–59.

Yu, Y., Chen, Z., Shi, L., Yang, F., Pan, J., Zhang, B., Sun, D., 2014. Anal. Chem. 86, 8200–8205.

Zhang, B., Liu, B., Chen, G., Tang, D., 2015a. Biosens. Bioelectron. 64, 6–12.

Zhang, P., Wu, X., Chai, Y., Yuan, R., 2014a. Analyst 139, 2748–2753.

Zhang, T., Lu, Y., Luo, G., 2014b. ACS Appl. Mater. Int. 6, 14433–14438.

Zhang, X., Wu, G., Cai, Z., Chen, X., 2015b. Talanta 134, 132–135.

Zheng, J., Ma, D., Shi, M., Bai, J., Li, Y., Yang, J., Yang, R., 2015. Chem. Commun. 51, 16271–16274.

Zhang, P., Wu, X., Yuan, R., Chai, Y., 2015. Anal. Chem. 87, 3202–3207.